Carter, L.B., Dasgupta, R., 2015, “Hydrous Basalt-Limestone Interaction at Crustal Conditions: Implications for Generation of Ultracalcic Melts nad Outflux of CO_2 at Volcanic Arcs,” Earth and Planetary Science Letters, doi: 10.1016/j.epsl.2015.06.

Supplementary Materials

Supplementary Table 1. Starting basalt composition as compared to hydrous starting materials in previous basalt-limestone interaction studies

	This Study	**F08**	**IM07**	**M10**	**J13**	**IM08**	**IM08**	**D10**
Starting Material	Primary arc basalt*	AH-7a plagioclase-free phonotephrite	AH7a potassic basalt	Primitive K-basalt	Primitive shoshonite	PST9 high-K calc-alkaline basalt	ST18 primitive shoshonite	M-94-a-107 basaltic-andesite
Source		Mt Mellone, Alban Hills, Italy	Mt Mellone, Alban Hills, Italy	Roman Province synthetic, Italy	Mt. Vesuvius, Italy	Stromboli, Italy	Stromboli, Italy	Mt Merapi, Indonesia
SiO_2	47.88	47.96	48.05	48.3	49.85(0.21)	50.38	52.07	51.83(0.43)
TiO_2	0.75	0.94	0.96	0.7	1.03(0.08)	0.86	0.93	0.89(0.05)
Al_2O_3	17.95	14.72	14.60	11.4	15.95(0.67)	15.36	16.71	18.08(0.24)
FeO_T	9.73	7.77	7.85	7.5	7.98(0.25)	7.91	7.61	8.17(0.16)
MnO	0.20	0.14	-	-	0.14(0.2)	-	-	-
MgO	5.99	6.38	6.45	13.7	6.03(0.33)	7.82	5.74	2.97(0.08)
CaO	10.97	11.32	11.40	14.0	9.98(0.29)	12.83	9.77	9.19(0.16)
Na_2O	2.00	1.67	1.63	1.2	2.35(0.07)	2.26	2.72	3.48(0.09)
K_2O	0.50	6.97	7.30	3.3	4.01(0.19)	1.91	3.65	2.05(0.03)
P_2O_5	-	0.50	0.51	-	0.7(0.09)	0.66	0.79	0.34(0.04)
Sum	95.97	98.97	98.75	100.1	98.02	97.48	97.83	97.2
$NaO+K_2O$	2.49	8.64	8.93	4.5	6.36	4.17	6.37	5.53
CaO/Al_2O_3	0.6	0.8	0.8	1.2	0.6	0.8	0.6	0.6
H_2O	4.03	0.7 to 1.7	1.25	1 and 5	0 to 2	1 to 6	1 to 6	2.23
Proportion of Carbonate	50	1 to 7	0 to 18	5 to 10	16.7 to 21.9	0 to 19	0 to 19	17 to 20

All values are in weight percent; for previous studies, number in (parentheses) are standard deviation where reported

FeO_T is total iron content ($FeO+Fe_2O_3$)

Primary arc basalt* composition determined based on weighed proportion of reagents (see Methods)

F08=Freda et al. (2008); IM07=Iacono-Marziano et al. (2007); M10=Mollo et al. (2010); J13=Jolis et al. (2013); IM08=Iacono Marziano et al. (2008); D10=Deegan et al. (2010)

Supplementary Table 2. Major element composition of experimental clinopyroxene (in wt.%)

Run no.	**B252***	**B291***	**B294***	**B292**	**B306**	**B293**	**B263**	**B274**	**B297**	**B264**	**B283**	**B266**	**B267**	**B295**	**B298**	**B280**
P (GPa)	**1.0**	**1.0**	**1.0**	**1.0**	**1.0**	**1.0**	**1.0**	**0.8**	**0.8**	**0.8**	**0.8**	**0.8**	**0.5**	**0.5**	**0.5**	**0.5**
T (°C)	**1100**	**1150**	**1175**	**1100**	**1150**	**1175**	**1200**	**1100**	**1125**	**1150**	**1175**	**1200**	**1100**	**1125**	**1150**	**1175**
n	7	7	9	13	7	9	7	8	8	6	5	7	2	4	9	5
SiO_2	47.5(8)	49.2(8)	48.1(8)	46(1)	49(2)	41.3(7)	41.6(5)	45.4(1)	46(1)	40.8(1)	41(2)	41(2)	37.7(3)	41(1)	39.5(1)	38.3(2)
TiO_2	0.61(9)	0.42(8)	0.40(4)	0.7(2)	0.8(2)	0.61(1)	0.7(2)	0.9(2)	0.74(8)	0.64(3)	0.7(2)	0.7(1)	0.63(9)	0.8(1)	0.71(6)	0.7(4)
Al_2O_3	7.9(9)	6.7(9)	6.9(8)	8(1)	7(2)	15.1(8)	18.0(9)	8.3(9)	10(1)	15(1)	15(2)	18(2)	15.9(2)	15(1)	15(1)	20(1)
FeO_T	12.0(7)	10.6(3)	8.7(3)	11.4(4)	11.5(6)	8.1(2)	8.0(2)	12.4(7)	10.3(3)	8.5(6)	9.5(9)	7.4(6)	11.0(9)	9.0(4)	9.6(1)	4.3(1)
MnO	0.40(5)	0.34(3)	0.27(5)	0.35(6)	0.37(7)	0.10(1)	0.14(5)	0.22(4)	0.22(6)	0.12(4)	0.10(4)	0.08(4)	0.10(2)	0.14(5)	0.16(4)	0.04(3)
MgO	13.2(5)	14.1(4)	14.4(5)	11.0(5)	12(2)	8.1(3)	7.7(4)	8.3(6)	10.7(1)	8.5(5)	8(1)	8.0(9)	7.9(2)	7.6(6)	7.3(4)	8.3(3)
CaO	17.1(8)	17.1(4)	18.8(3)	19(1)	17(2)	23.9(2)	24.2(2)	23.6(4)	21(1)	23.9(3)	23.3(6)	24.5(2)	25.2(2)	25.1(4)	26(1)	24.8(3)
Na_2O	0.64(4)	0.54(4)	0.59(5)	0.72(6)	0.7(2)	0.44(8)	0.32(4)	0.25(6)	0.6(2)	0.30(7)	0.19(6)	0.22(5)	0.06(3)	0.22(9)	0.2(1)	0.07(5)
K_2O	0.012(9)	0.002(4)	0.02(1)	0.01(1)	0.1(2)	0.012(9)	0.004(4)	0.006(9)	0.04(7)	0.005(5)	0.011(8)	0.003(4)	#NUM!	0.02(2)	0.03(2)	0.006(8)
Sum	99.2(5)	99.0(6)	98.3(6)	98(2)	99(1)	97.7(7)	100.6(8)	99.4(5)	99.2(7)	97.8(5)	97.2(8)	99.4(3)	98.5(7)	99.0(6)	97.8(9)	96.4(7)
Fs+En	65	66	63	58	63	38	35	48	53	39	41	33	45	39	42	24
Wo	24	25	24	30	29	36	38	39	31	34	35	38	25	35	30	36
CaTs	11	9	13	12	8	26	26	13	16	27	23	28	30	26	28	40
Total	100	100	100	100	100	100	99	100	100	100	100	99	100	100	100	100

*Experiments with starting hydrous basalt composition only; all others performed with 50 wt.% basalt and 50 wt.% calcite

Number in (parentheses) is one sigma standard deviation for *n* number of EMPA spot analyses averaged for each phase reported in least digits cited, i.e., 47.5(8) should be read as 47.5 ± 0.8 wt.%

FeO_T is total iron content ($FeO+Fe_2O_3$)

End-members (En=enstatite, Fs=ferrosilite, Wo=wollastonite, CaTs=Ca-Tschermak) in % by atomic proportion

Supplementary Table 3. Major element composition of experimental plagioclase (in wt.%)

Run no.	B252*	B291*	B294*	B292	B306	B274	B297	B283	B267	B295	B298
P (GPa)	1.0	1.0	1.0	1.0	1.0	0.8	0.8	0.8	0.5	0.5	0.5
T (°C)	1100	1150	1175	1100	1150	1100	1125	1175	1100	1125	1150
n	4	4	8	3	4	6	10	8	8	5	5
SiO_2	51.8(1)	50(1)	50.0(9)	49.9(5)	53(1)	51(1)	51(1)	50.9(5)	48(2)	49(1)	52.7(9)
TiO_2	-	0.2(1)	0.05(5)	0.3(1)	0.2(1)	0.15(9)	0.09(6)	0.06(4)	0.5(2)	0.23(5)	0.09(2)
Al_2O_3	30(1)	28(1)	30.0(5)	27(2)	29.9(9)	28.6(9)	30.5(9)	31.1(3)	25(3)	30.5(9)	28.3(5)
FeO_T	2.1(4)	3(2)	0.9(2)	2.4(7)	1.2(6)	1.3(4)	1.3(4)	0.9(1)	3(1)	1.5(2)	0.9(1)
MnO	-	0.07(5)	0.02(2)	0.10(5)	0.02(2)	0.06(6)	0.04(3)	0.02(2)	0.14(7)	0.09(3)	0.02(1)
MgO	0.4(2)	1.0(7)	0.2(2)	0.7(2)	0.2(2)	0.3(1)	0.17(8)	0.10(5)	0.9(4)	0.32(5)	0.2(2)
CaO	12.6(2)	13.2(5)	14.2(4)	12.3(4)	13(1)	12.9(9)	14.1(9)	13.9(5)	18.0(8)	16.3(7)	12(1)
Na_2O	3.5(3)	3.1(5)	3.4(2)	3.4(2)	3.3(3)	3.6(3)	3.4(6)	3.2(2)	3.1(5)	2.8(4)	4.6(4)
K_2O	0.26(5)	0.21(3)	0.13(2)	0.4(1)	0.3(2)	0.6(2)	0.25(8)	0.22(3)	0.9(3)	0.32(8)	0.42(4)
Sum	100(2)	99(1)	98.8(7)	96(1)	101.1(7)	100(1)	99.4(3)	100(2)	100(8)	101(4)	99(3)
An	49	53	53	48	51	47	53	53	57	60	41
Ab	49	45	46	48	46	48	45	45	36	37	56
Or	2	2	1	4	3	5	2	2	7	3	3
Total	100	100	100	100	100	100	100	100	100	100	100

*Experiments with starting hydrous basalt composition only; all others performed with 50 wt.% basalt and 50 wt.% calcite
Number in (parentheses) is one sigma standard deviation for *n* number of EMPA spot analyses averaged for each phase reported in least digits cited, i.e., 51.8(1) should be read as 51.8 ± 0.1 wt.%
FeO_T is total iron content ($FeO+Fe_2O_3$)
End-members (Ab=albite, An=anorthite, Or=orthoclase) in % by atomic proportion of Na^{2+}, Ca^{2+}, and K^+, respectively.

Supplementary Table 4. Major element composition of experimental scapolite (in wt.%)

Run no.	**B306**	**B293**	**B263**	**B297**	**B264**	**B283**	**B266**	**B295**	**B298**
P (GPa)	**1.0**	**1.0**	**1.0**	**0.8**	**0.8**	**0.8**	**0.8**	**0.5**	**0.5**
T (°C)	**1150**	**1175**	**1200**	**1125**	**1150**	**1175**	**1200**	**1125**	**1150**
n	4	7	10	5	7	4	4	7	5
SiO_2	43(3)	40.6(5)	37(1)	37.4(9)	37.4(9)	41(1)	39.8(3)	40.4(5)	39(1)
TiO_2	0.05(2)	0.02(2)	0.03(2)	0.03(2)	0.03(2)	0.04(3)	0.03(3)	0.02(1)	0.03(3)
Al_2O_3	30(3)	29.3(3)	29.4(9)	26.1(8)	26.1(8)	29.0(8)	30.7(2)	30.8(5)	31.3(8)
FeO_T	0.8(1)	0.6(1)	0.51(5)	1.0(2)	1.0(2)	0.59(9)	0.62(5)	0.49(3)	0.7(1)
MnO	0.03(1)	0.03(3)	0.02(3)	0.02(2)	0.02(2)	0.01(2)	0.02(2)	0.02(2)	0.01(1)
MgO	0.2(1)	0.14(1)	0.17(2)	0.18(8)	0.18(8)	0.15(2)	0.16(3)	0.17(2)	0.13(5)
CaO	21(1)	21.9(4)	21.8(4)	22.8(4)	22.8(4)	21.1(5)	22.4(1)	22.2(3)	22.8(9)
Na_2O	1.1(7)	1.0(2)	0.86(5)	0.8(2)	0.8(2)	1.5(3)	0.47(4)	0.73(9)	0.4(1)
K_2O	0.12(5)	0.07(1)	0.06(2)	0.06(4)	0.06(4)	0.11(1)	0.04(2)	0.05(2)	0.02(2)
Est. CO_2[a]	4(1)	6.4(1)	10(2)	12(2)	12(2)	6(2)	5.8(6)	5(1)	5.6(9)
Sum	98.4(5)	100.3(6)	100.4(4)	100.8(8)	100.8(8)	100(5)	100(1)	100(2)	100(4)
Eq An	95	93	93	94	94	89	96	94	97
% Me (S60)	95	92	93	94	94	89	96	94	97
% Me (E69)	83	84	92	80	80	81	91	89	95

Number in (parentheses) is one sigma standard deviation for *n* number of EMPA spot analyses averaged for each phase reported in least digits cited, i.e., 43(3) should be read as 43 ± 3 wt.%

FeO_T is total iron content ($FeO+Fe_2O_3$)

Est. CO_2[a] is estimated stoichiometrically, normalized to (Al+Si)=12 cations

Eq An=Equivalent Anorthite content calculated after the method of Moecher and Essene (1990)

% Me (E69)=percent Meionite following the method of Evans et al. (1969); % Me (S60)=percent Meionite following the method of Shaw (1960) (see Supplementary Fig. 1).

Carter, L.B., Dasgupta, R., 2015, “Hydrous Basalt-Limestone Interaction at Crustal Conditions: Implications for Generation of Ultracalcic Melts nad Outflux of CO_2 at Volcanic Arcs,” Earth and Planetary Science Letters, doi: 10.1016/j.epsl.2015.06.

Supplementary Fig. 1. Experimental scapolites analyzed in this study (following the symbols used in Fig. 5) plotted by Equivalent Anorthite content (Eq An; [Al-3]/3*100) after Moecher and Essene (1990) and by Meiorite content (% Me) following the equation of Evans *et al.* (1969; Ca/[Ca+Na+K]*100). The insert shows the close 1:1 correspondence between this method and that of Shaw (1960; [Ca+Mg+Fe+Mn+Ti]/[Na+K+Ca+Mg+Fe+Mn+Ti]*100). Natural data are from compilations of scapolite analyses (open circles – Shaw, 1960: Helsinki, USA (Massachusetts, Pennsylvania, New York, New Hampshire), Canada (Ontario and Quebec), the former USSR, Italy (Vesuvius), Finland, Sweden, Norway, Germany (Laacher See), Austria, Moravia; x – Harley and Buick, 1992: Antarctica; closed circles – Evans *et al.*, 1969: Tanzania, USA (Massachusetts, Pennsylvania, New York), and Italy (Somma-Vesuvius); crosses – Pan *et al.*, 1994: Canada; dashes – Yoshino and Satish-Kumar, 2001: the Himalayas).

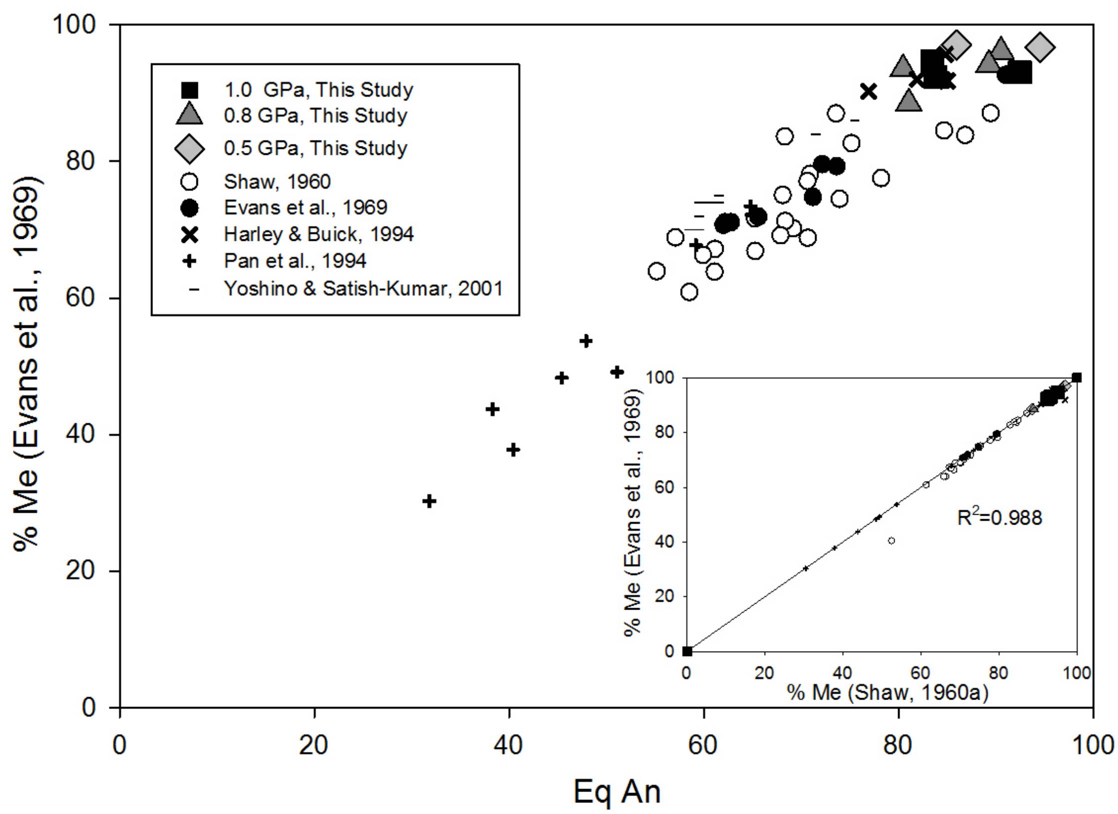

Additional reference information for Fig. 7

Data for natural ultracalcic melt inclusions shown as the grey region were collected from: 1) Batan Island, Philippines (Schiano et al., 2000); 2) Iceland (Sigurdsson et al., 2000); 3) 43ºN (Kamenetsky et al., 1998); 4) Bulgaria (Marchev et al., 2009); 5) Tonga arc (Falloon and Green, 1986); 6) Srednogorie arc, SW Europe (Georgiev et al., 2009). Previous carbonate assimilation experiments performed at 0.5 GPa (labeled 'C09' and 'IM09') from Conte et al. (2009) and Iacono Marziano et al. (2008) are plotted as open and closed circles, respectively. The ultracalcic melts of Mollo and Vona (2014) are similar but not plotted for comparison as they were performed at atmospheric pressures. Experimental lherzolite data ('+' symbols, labeled 'G04' and 'S04') are compiled from (Green et al., 2004; Schmidt et al., 2004) and wehrlite data ('x' symbols, labeled 'M06') from the experiments of (Medard, 2006).

Oxygen fugacity determination

It has been speculated that preferential incorporation of Al^{3+} for Si^{4+} in the tetrahedral site in cpx, seen with increasing assimilation in this study, is perhaps influenced by an enhanced incorporation of Fe^{3+} in the cpx, owing to oxidative capacity of CO_2, following the reaction such as:

$$CO_2\,(\text{fluid}) + 2FeO\,(\text{melt}) = CO\,(\text{fluid}) + Fe_2O_3\,(\text{melt}) \quad \text{(Supplementary Eq. 1)}$$

(Conte *et al.*, 2009; Mollo and Vona, 2014b and references therein). Oxygen fugacity of our experiments were not buffered, but the estimated oxygen fugacity within the capsules, calculated using the equilibrium between iron content dissolved by the AuPd capsule and FeO content of coexisting silicate glass, was higher when calcite was present at 1.0 GPa, 1200 °C (ΔFMQ +1.8 ± 0.2 or 2.8 ± 0.1 with calcite; ΔFMQ +1.4 ± 0.3 or 2.4 ± 0.3 without calcite, following to the fO_2 parameterizations of Barr and Grove, 2010 and Balta *et al.*, 2011 respectively). Using the model of Barr and Grove (2010) who determined and included a temperature-dependence with their empirical equation, we calculate an increase in oxygen fugacity with increased calcite consumption at higher temperatures (ΔFMQ -0.30±0.1 at 1100 °C; ΔFMQ + 0.41 ± 0.1 at 1200 °C, 0.5 GPa, Table 1). Additionally, Fe_2O_3/FeO_T in cpx grains was estimated using atomic site assignment calculations. The ratio of ferric to total iron rapidly increases with calcite presence (0.30 without calcite; 0.49 with calcite at 1.0 GPa, 1100 °C) and with increasing temperature and decreasing pressure in calcite-bearing experiments (as much as ~1.00 at 0.5 GPa, 1175 °C). Thus our experimental determination of fO_2 is broadly in agreement with the notion that increased CO_2 release by carbonate assimilation can also lead to oxidation of the silicate subsystem, thereby promoting formation of more CaTs-rich clinopyroxenes.

References

Balta, J.B., Beckett, J.R., Asimow, P.D., 2011. Thermodynamic properties of alloys of gold-74/palladium-26 with variable amounts of iron and the use of Au-Pd-Fe alloys as containers for experimental petrology. Am. Mineral. 96, 1467–1474. doi:10.2138/am.2011.3637

Barr, J.A., Grove, T.L., 2010. AuPdFe ternary solution model and applications to understanding the fO_2 of hydrous, high-pressure experiments. Contrib. to Mineral. Petrol. 160, 631–643. doi:10.1007/s00410-010-0497-z

Conte, A.M., Dolfi, D., Gaeta, M., Misiti, V., Mollo, S., Perinelli, C., 2009. Experimental constraints on evolution of leucite-basanite magma at 1 and 10^{-4} GPa: implications for parental compositions of Roman high-potassium magmas. Eur. J. Mineral. 21, 763–782. doi:10.1127/0935-1221/2009/0021-1934

Deegan, F.M., Troll, V.R., Freda, C., Misiti, V., Chadwick, J.P., McLeod, C.L., Davidson, J.P., 2010. Magma-Carbonate Interaction Processes and Associated CO2 Release at Merapi Volcano, Indonesia: Insights from Experimental Petrology. J. Petrol. 51, 1027–1051. doi:10.1093/petrology/egq010

Evans, B.W., Shaw, D.M., Haughton, D.R., 1969. Scapolite stoichiometry. Contrib. to Mineral. Petrol. 24, 293–305. doi:10.1007/BF00371272

Falloon, T., Green, D., 1986. Glass inclusions in magnesian olivine phenocrysts from Tonga: evidence for highly refractory parental magmas in the Tongan arc. Earth Planet. Sci. Lett. 81, 95–103.

Freda, C., Gaeta, M., Misiti, V., Mollo, S., Dolfi, D., Scarlato, P., 2008. Magma–carbonate interaction: An experimental study on ultrapotassic rocks from Alban Hills (Central Italy). Lithos 101, 397–415. doi:10.1016/j.lithos.2007.08.008

Carter, L.B., Dasgupta, R., 2015, “Hydrous Basalt-Limestone Interaction at Crustal Conditions: Implications for Generation of Ultracalcic Melts nad Outflux of CO_2 at Volcanic Arcs,” Earth and Planetary Science Letters, doi: 10.1016/j.epsl.2015.06.

Georgiev, S., Marchev, P., Heinrich, C. a., Von Quadt, a., Peytcheva, I., Manetti, P., 2009. Origin of Nepheline-normative High-K Ankaramites and the Evolution of Eastern Srednogorie Arc in SE Europe. J. Petrol. 50, 1899–1933. doi:10.1093/petrology/egp056

Green, D.H., Schmidt, M.W., Hibberson, W.O., 2004. Island-arc Ankaramites: Primitive Melts from Fluxed Refractory Lherzolitic Mantle. J. Petrol. 45, 391–403. doi:10.1093/petrology/egg101

Harley, S., Buick, I., 1992. Wollastonite—Scapolite Assemblages as Indicators of Granulite Pressure-Temperature-Fluid Histories: The Rauer Group, East Antarctica. J. Petrol. 33, 693–728.

Iacono-Marziano, G., Gaillard, F., Pichavant, M., 2007. Limestone assimilation and the origin of CO_2 emissions at the Alban Hills (Central Italy): Constraints from experimental petrology. J. Volcanol. Geotherm. Res. 166, 91–105. doi:10.1016/j.jvolgeores.2007.07.001

Iacono-Marziano, G., Gaillard, F., Pichavant, M., 2008. Limestone assimilation by basaltic magmas: an experimental re-assessment and application to Italian volcanoes. Contrib. to Mineral. Petrol. 155, 719–738. doi:10.1007/s00410-007-0267-8

Jolis, E.M., Freda, C., Troll, V.R., Deegan, F.M., Blythe, L.S., McLeod, C.L., Davidson, J.P., 2013. Experimental simulation of magma–carbonate interaction beneath Mt. Vesuvius, Italy. Contrib. to Mineral. Petrol. 166, 1335–1353. doi:10.1007/s00410-013-0931-0

Kamenetsky, V.S., Eggins, S.M., Crawford, A.J., Green, D.H., Gasparon, M., Falloon, T.J., 1998. Calcic melt inclusions in primitive olivine at 43°N MAR: evidence for melt–rock reaction/melting involving clinopyroxene-rich lithologies during MORB generation. Earth Planet. Sci. Lett. 160, 115–132. doi:10.1016/S0012-821X(98)00090-9

Marchev, P., Georgiev, S., Zajacz, Z., Manetti, P., Raicheva, R., von Quadt, A., Tommasini, S., 2009. High-K ankaramitic melt inclusions and lavas in the Upper Cretaceous Eastern Srednogorie continental arc, Bulgaria: Implications for the genesis of arc shoshonites. Lithos 113, 228–245. doi:10.1016/j.lithos.2009.03.014

Medard, E., 2006. Melting of Amphibole-bearing Wehrlites: an Experimental Study on the Origin of Ultra-calcic Nepheline-normative Melts. J. Petrol. 47, 481–504. doi:10.1093/petrology/egi083

Moecher, D., Essene, E., 1990. Phase Equilibria for Calcic Scapolite, and Implications of Variable Al-Si Disorder for PT, T-X_{CO2}, and aX Relations. J. Petrol. 31, 997–1024.

Mollo, S., Gaeta, M., Freda, C., Di Rocco, T., Misiti, V., Scarlato, P., 2010. Carbonate assimilation in magmas: A reappraisal based on experimental petrology. Lithos 114, 503–514. doi:10.1016/j.lithos.2009.10.013

Mollo, S., Vona, a., 2014. The geochemical evolution of clinopyroxene in the Roman Province: A window on decarbonation from wall-rocks to magma. Lithos 192-195, 1–7. doi:10.1016/j.lithos.2014.01.009

Carter, L.B., Dasgupta, R., 2015, “Hydrous Basalt-Limestone Interaction at Crustal Conditions: Implications for Generation of Ultracalcic Melts nad Outflux of CO_2 at Volcanic Arcs,” Earth and Planetary Science Letters, doi: 10.1016/j.epsl.2015.06.

Pan, Y., Fleet, M., Ray, G., 1994. Scapolite in two Canadian gold deposits; Nickel Plate, British Columbia and Hemlo, Ontario. Can. Mineral. 32, 825–837.

Schiano, P., Eiler, J.M., Hutcheon, I.D., Stolper, E.M., 2000. Primitive CaO-rich, silica-undersaturated melts in island arcs: Evidence for the involvement of clinopyroxene-rich lithologies in the petrogenesis of arc magmas. Geochemistry, Geophys. Geosystems 1, 1–33. doi:10.1029/1999GC000032

Schmidt, M.W., Green, D.H., Hibberson, W.O., 2004. Ultra-calcic Magmas Generated from Ca-depleted Mantle: an Experimental Study on the Origin of Ankaramites. J. Petrol. 45, 531–554. doi:10.1093/petrology/egg093

Shaw, D.M., 1960. The Geochemistry of Scapolite Part I. Previous Work and General Mineralogy. J. Petrol. 1, 218–260. doi:10.1093/petrology/1.1.218

Sigurdsson, I., Steinthorsson, S., Grönvold, K., 2000. Calcium-rich melt inclusions in Cr-spinels from Borgarhraun, northern Iceland. Earth Planet. Sci. Lett. 183, 15–26.

Yoshino, T., Satish-Kumar, M., 2001. Origin of scapolite in deep-seated metagabbros of the Kohistan Arc, NW Himalayas. Contrib. to Mineral. Petrol. 140, 511–531. doi:10.1007/s004100000207